energies

MDPI

Article

Novel Single-Phase Short-Stroke Tubular Permanent Magnet Oscillating Machines with Partitioned Stator

Zi-Qiang Zhu [1,*], Ahlam Luaibi Shuraiji [2], Qinfen Lu [3], Yanxin Li [3] and Huan Qu [1]

[1] Department of Electronic and Electrical Engineering, University of Sheffield, Sheffield S1 3JD, UK; hqu2@sheffield.ac.uk
[2] Electromechanical Engineering Department, University of Technology Baghdad, Baghdad 00964, Iraq; ahlamly2009@yahoo.com
[3] College of Electrical Engineering, Zhejiang University, Hangzhou 310027, China; luqinfen@zju.edu.cn (Q.L.); eeliyanxin@zju.edu.cn (Y.L.)
* Correspondence: Z.Q.Zhu@sheffield.ac.uk; Tel.: +44-114-222-5360

Abstract: This paper presents three novel configurations of single-phase (SP) short-stroke (SS) tubular permanent magnet oscillating machines (TPMOMs) with partitioned stator (PS), termed PS-SPSS-TPMOMs. The machine structures are described and the influence of permanent magnet pole alignment with either stator slot or stator tooth is investigated. It is found that the PM poles should be aligned with the stator slots in order to ease the oscillation. The electromagnetic performance of these proposed machines is analyzed and compared. The results show that such machines have the advantages of low mover mass and low magnet eddy current loss, compared with a conventional surface-mounted SPSS-TPMOM.

Keywords: cogging force; partitioned stator; permanent magnet; single phase; tubular machine

Citation: Zhu, Z.-Q.; Shuraiji, A.L.; Lu, Q.; Li, Y.; Qu, H. Novel Single-Phase Short-Stroke Tubular Permanent Magnet Oscillating Machines with Partitioned Stator. *Energies* **2021**, *14*, 1863. https://doi.org/10.3390/en14071863

Academic Editor: Yacine Amara

Received: 18 February 2021
Accepted: 24 March 2021
Published: 27 March 2021

1. Introduction

Linear oscillating machines that control linear reciprocating motion through stroke cycles at a specific frequency have the merits of high transmission efficiency, simple structure, and low noise and vibration. For every rotary electrical machine, there exists a linear counterpart, and hence various linear induction machines [1–3], linear switched reluctance machines [4–6], and linear permanent magnet PM machines [7–10] have been developed.

Recently, tubular PM machines have been proposed for transportation, military, and industrial applications, etc. [11]. This is due to the fact that such machines combine the merits of PM machines, e.g., high torque density and high power densities [12], and the advantages of tubular structures, i.e., no end winding effect and no normal force [13]. It was reported that tubular PM machines deliver higher force and higher power densities than other linear PM machine topologies. Consequently, the highest efficiency can be achieved [14].

Generally, tubular PM machines can be categorized according to whether their mover is iron or magnet. By considering the mover traveling displacement, tubular PM machines are divided into short-stroke and long-stroke machines [15]. The interest in single-phase short-stroke tubular PM machines (SPSS-TPMMs) has been considerably increasing over the last few years, and they have been applied in healthcare [16], wave energy extraction [17], and household appliances [18]. This is because single-phase tubular machines are particularly suitable for short-stroke operation, require simpler control, and are less affected by flux fringing effects compared with their three-phase counterparts [19,20].

As a promising candidate for refrigerator compressor applications, an SPSS-TPMM was presented in [18]. The machine comprises a C-core stator and a two-pole PM Halbach magnetized mover. It has been demonstrated that the machine can offer good performance

with an efficiency of around 93%. On the other hand, [21] investigated the effect of the main design parameters on an SPSS-TPMM's efficiency, and an approach to achieve the maximum machine efficiency was described.

Furthermore, to reduce the eddy current loss and minimize the moving mass, the aforementioned machine was redesigned with a non-ferromagnetic back-iron mover in [22]. Such a machine has the advantage of low mover mass, which enhances the dynamic capability. However, it shows less efficiency than a machine with a ferromagnetic back-iron mover. The influence of winding configurations on the aforementioned machine's performance was introduced in [23]. It has been concluded that a machine with a C-core has a higher thrust force than that with distributed winding. The authors of [24] introduced a new magnet configuration and the magnet shape was changed into a trapezoid instead of a rectangular shape. The influence of split ratio, PM angle, and axial magnet width to pole pitch ratio on the machine loss and efficiency was examined. An E-core stator, Halbach magnetized PM mover SPSS-TPMM was designed and analyzed in [25]. The radial magnet width to pole pitch ratio was optimized for maximum thrust force, and the optimal combination of stator tooth and mover pole numbers was determined. It was confirmed that the difference between the stator tooth number and the mover pole number should be equal to one. In [26], a comparison of E- and C-core SPSS-TPMMs with radial, axial, and Halbach magnetized PM movers was presented. It was found that a C-core machine with an axially magnetized magnet mover produces a similar peak thrust force as one with an E-core Halbach magnetized PM mover, while the magnet usage is halved. Since the Halbach magnetized PM mover performs better among these types, more in-depth investigations on this topic have been presented [27,28]. Furthermore, the replacement of expensive rare-earth magnets has been attempted. It has been confirmed that the performance is comparable for machines with more economic ferrite magnets [29].

Although all the abovementioned machines exhibit high thrust force, such topologies suffer from thermal dissipation difficulty. A simple rotor structure may be considered as one of the main distinguished features of the doubly salient PM machines that have both excitation sources in the stator [30–35]. A switched flux SPSS-TPMOM (SF-SPSS-TPMOM) has been designed [36], and the influence of leading design parameters on the machine's performance was investigated. The machine has a simple and robust mover. However, it exhibits less power density compared with the conventional PM mover counterpart. Thus, a dual-stator SF-SPSS-TPMOM was introduced to enhance the power density of the single-stator SF-SPSS-TPMOM. The machine comprises two stators having identical mechanical structures. Each stator consists of a C-core with annular winding and two PMs oppositely magnetized in the axial direction, while the mover is yokeless and made of two iron pieces. It has been observed that better performance with lower mover mass can be obtained for a dual-stator machine compared with a single-stator machine. However, the magnet volume is increased. Recently, a new topology so-called a partitioned stator PM machine in which each excitation source is placed in separated stators has been designed [37]. It was demonstrated that better inner space utilization can be achieved, and the difficulty of PM heat dissipation, as well as the conflict of electric and magnetic loadings, can be overcome with forced cooling.

In this paper, three novel SPSS-TPMOMs with surface-mounted and interior PMs are proposed, and the concept of a partitioned stator is adopted (known as PS-SPSS-SPMTM and PS-SPSS-IPMTM). The machine structures are described in Section 2, while the influence of the PM pole alignment with either stator slot or stator tooth is investigated in Section 3. Furthermore, the main design parameters of the proposed machines are optimized in Section 4. Section 5 provides the machine performance analysis and comparison. Section 6 focuses on the loss analysis and comparison. A conventional single-phase short-stroke surface-mounted PM tubular machine is then used for comparison with its partitioned-stator counterpart in Section 7. Finally, the conclusions are presented in Section 8.

2. Machine Configurations

The proposed machines consist of two stators and one mover. The outer stator is designed with an E-core and two annular windings having opposite current directions. The PMs are located on the inner stator, while the iron pieces of the mover are sandwiched between the two stators. The difference among the three proposed machine configurations is the PM location, i.e., on the surface of the inner stator with radial magnetization for PS-SPSS-SPMTM, and embedded in the inner stator iron with axial magnetization for the PS-SPSS-IPMTM. It should be emphasized that the PS-SPSS-IPMTM is designed with two configurations, i.e., PS-SPSS-IPMTM-1 with one magnet pole and PS-SPSS-IPMTM-2 with two magnet poles. Figures 1 and 2 show the 3D and 2D views of the proposed machine topologies. The design specifications are listed in Table 1.

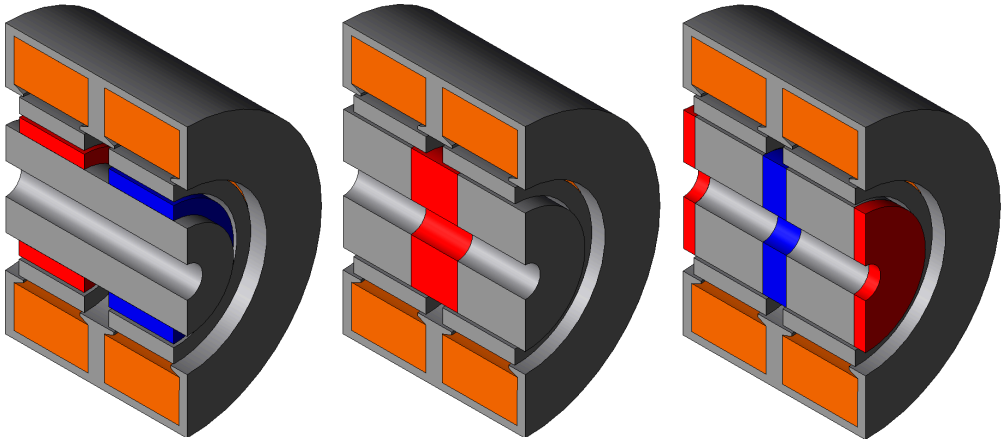

(**a**) (**b**) (**c**)

Figure 1. Three-dimensional views of proposed machine topologies with an inner space for assembly. (**a**) Partitioned stator single-phase short-stroke surface-mounted permanent magnet tubular machine (PS-SPSS-SPMTM); (**b**) Partitioned stator single-phase short-stroke interior permanent magnet tubular machine 1 (PS-IPSS-SPMTM-1); (**c**) Partitioned stator single-phase short-stroke interior permanent magnet tubular machine 2 (PS-SPSS-IPMTM-2).

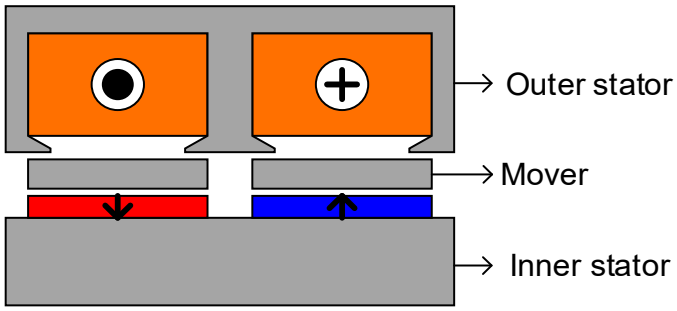

(**a**)

Figure 2. *Cont*.

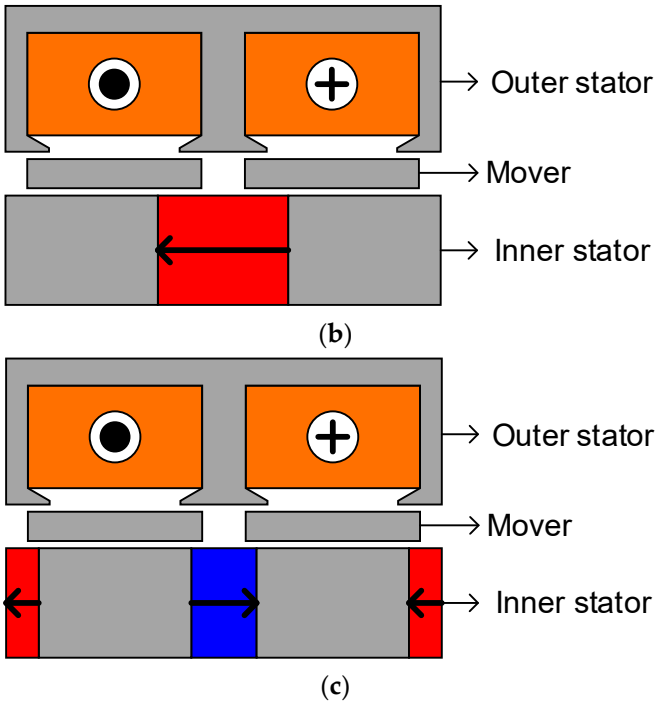

Figure 2. Two-dimensional views of proposed machine topologies. (**a**) PS-SPSS-SPMTM; (**b**) PS-IPSS-SPMTM-1; (**c**) PS-SPSS-IPMTM-2.

Table 1. Machines' main design parameters.

Items	Values
Outer radius (mm)	35
Machine active length (mm)	47.2
Inner air gap length (mm)	0.8
Outer air gap length (mm)	0.8
Slot number	2
Pole number	2
Current density (A/mm^2)	4
Turns per coil	350
Remanence of magnet (T)	1.2
Recoil permeability of magnet	1.05

3. Influence of Permanent Magnet Alignment

To obtain a proper design of the proposed machines, which should be able to produce oscillation, the influence of PM pole alignment with either stator slot or stator tooth will be investigated in this section. Two configurations for each machine are designed as shown in Figure 3. It is worth mentioning that model 1 refers to the PS-SPSS-SPMTM where the PM poles are aligned with stator teeth, while the PS-SPSS-SPMTM in which the PM poles align with the stator slots is designated as model 2. On the other hand, model 3 and model 4 represent PS-SPSS-IPMTMs where the PM poles are designed to align with stator teeth and stator slots, respectively. It has been proven that to achieve oscillation, the profile of the back electromotive force (back-EMF) with the mover displacement for the SPSS-SPMTM must not be bipolar [38]. Therefore, the no-load performances of the aforementioned machines are analyzed and compared. Flux linkage and back-EMF variations with the mover displacement of the two configurations are compared in Figures 4 and 5, respectively. For the sake of ease of comparison, the mover will run at a constant speed within the operation range. It can be seen that the flux linkage of model 1 is unipolar with the variation in mover position, resulting in bipolar back-EMF with the displacement. Thereby, such a configuration is incapable of producing oscillation [38]. In contrast, bipolar flux linkage varies with

the mover displacement, leading to a unipolar back-EMF displacement characteristic in model 2. Thus, oscillation can be achieved with this topology. Moreover, Figure 5 shows the variations in the flux linkage and the back-EMF with the mover displacement of model 3 and model 4, respectively. Model 3 cannot achieve oscillation due to the bipolar profile of its back-EMF against the mover displacement, whereas model 4 exhibits a unipolar back-EMF displacement characteristic and oscillation can be obtained. According to the above analysis, it can be concluded that the PM poles should be aligned with stator slots for PS-SPSS-TPMOMs.

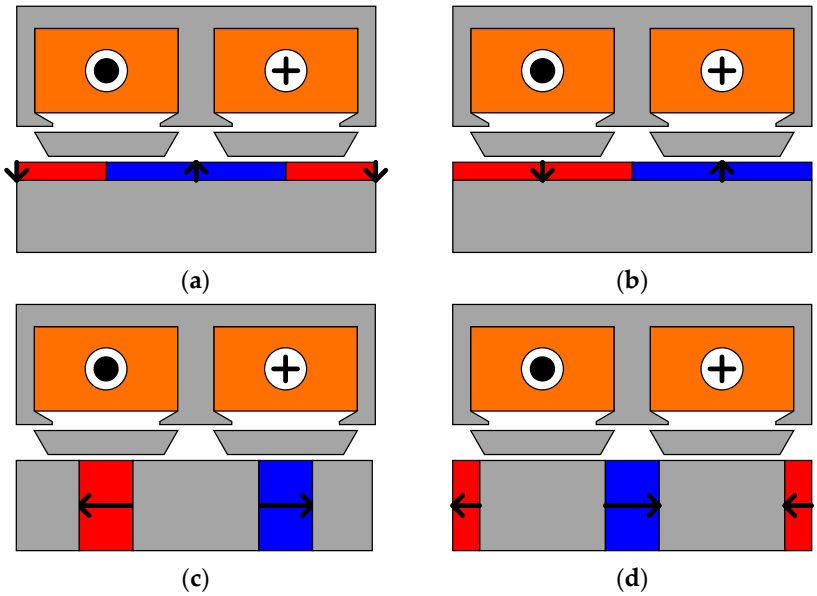

Figure 3. Analyzed machines. (**a**) Model 1; (**b**) Model 2; (**c**) Model 3; (**d**) Model 4.

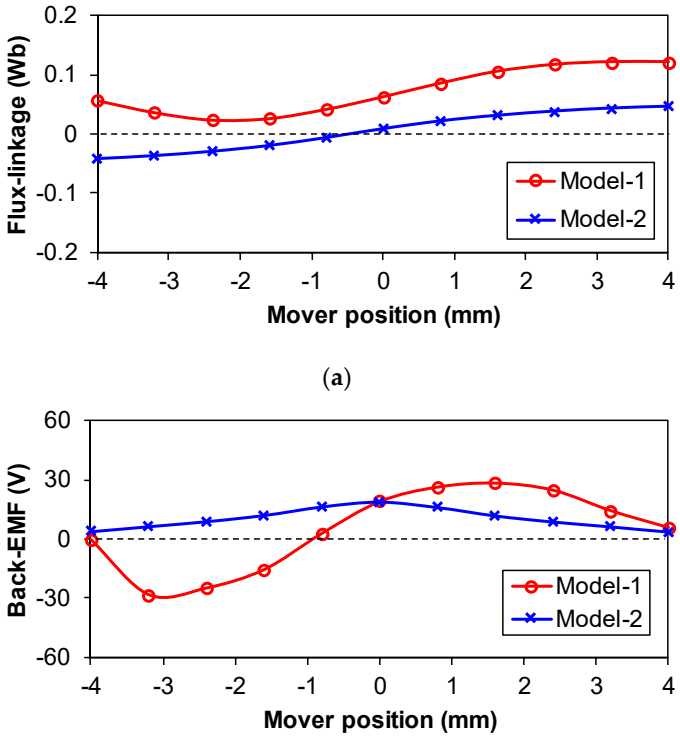

Figure 4. Comparison of PS-SPSS-SPMTM models. (**a**) Flux linkages; (**b**) Back-EMFs.

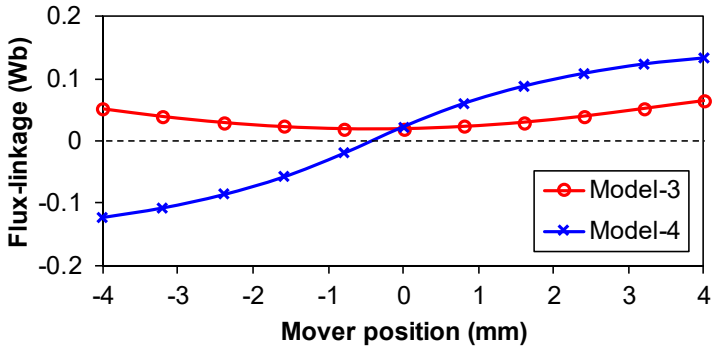

(**a**)

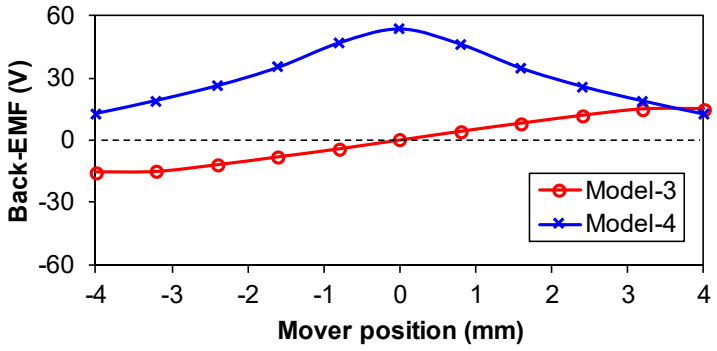

(**b**)

Figure 5. Comparison of PS-SPSS-IPMTM models. (**a**) Flux linkages; (**b**) Back-EMFs.

4. Machine Optimization

Global optimization based on a genetic algorithm and finite element model has become a prevalent technique in machine design optimization. Hence, this section presents the global optimization of machines for maximum thrust force. The outer radius, the machine active length, and the current density are kept constant during the optimization. The parameters, which are varied during this optimization process, are defined in Table 2, while the main design parameters are illustrated in Figure 6. The objective of the global optimization is to obtain the maximum average thrust force value with the initial and restriction values of the machine parameters, which are listed in Table 3. The genetic algorithm parameters are set up as follows: population size and maximum generation are 20; crossover type is simulated binary crossover; individual crossover probability, variable crossover probability, and the related parameter Mu have the value of 1; variable exchange probability has the value of 0; mutation type is chosen to be polynomial mutation; the uniform mutation probability takes 0; variable mutation probability and individual mutation probability are 1; and the standard deviation is 0.05. Table 3 presents the initial, constrain, and optimal values of the design parameters that are optimized for maximum thrust force.

Table 2. Definition of optimization parameters.

Symbols	Definitions	Expressions
SR	Split ratio	MGO */OSR
TMPWR	Top mover pole pitch width ratio	TMPW/MPP
BMPWR	Bottom mover pole pitch width ratio	BMPW/MPP
OSTWR	Outer stator tooth width ratio	OSTW/OSSP
OSSOR	Outer stator slot opening ratio	OSSO/OSSP
OSBITHR	Outer stator back iron thickness ratio	OSBITH/OSTH
TPMR	PM pole ratio	TPM/ISPP

* MGO = ISR + GI + MTH + GO/2, where MTH, TMPW, BMPW, and MPP are the radial thickness, the top piece width, the bottom piece width, and the pole pitch of the mover, respectively. OSTW, OSSO, OSBITH, OSTH, and OSSP indicate the tooth width, the slot opening, the back iron thickness, the total height, and the slot pitch of the outer stator, respectively. ISR, ISBITH, and ISPP represent the radius and pole pitch of the inner stator, respectively, while TPM is the magnet pitch. GI and GO refer to the inner and outer air gaps, respectively.

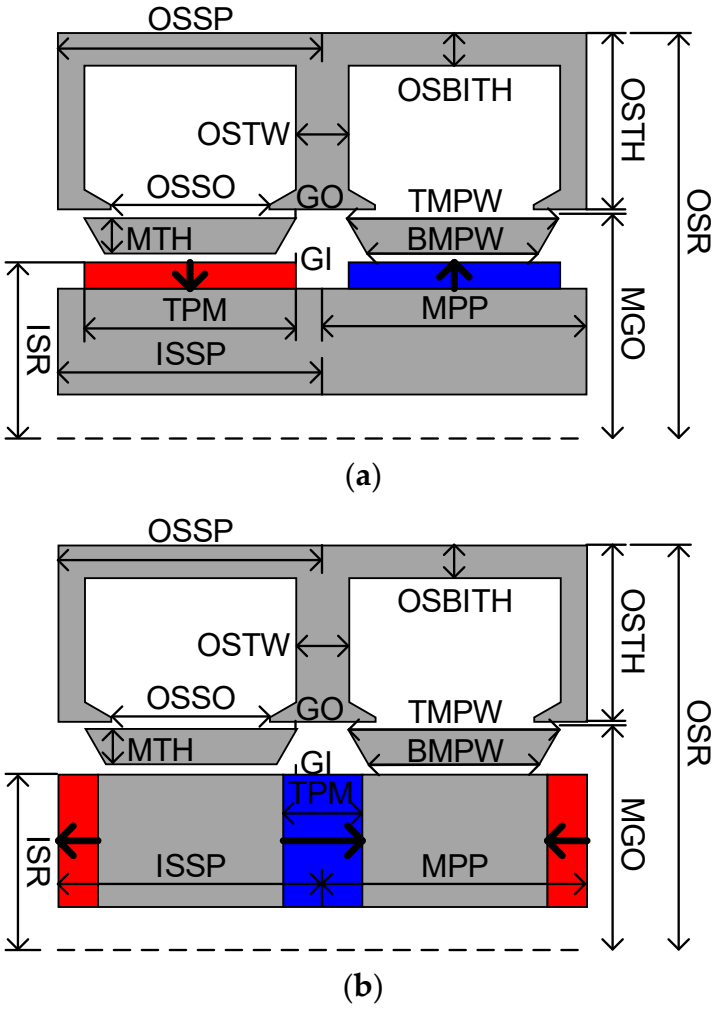

Figure 6. Main design parameters. (**a**) PS-SPSS-SPMTM; (**b**) PS-SPSS-IPMTM.

Table 3. Values of optimization parameters.

Symbols	Initials	Restrictions	PS-SPSS-SPMTM	Optimal PS-SPSS-IPMTM-1	PS-SPSS-IPMTM-2
SR	0.5	[0.3, 0.75]	0.58	0.6	0.58
TMPWR	0.8	[0.3, 0.9]	0.73	0.75	0.85
BMPWR	0.6	[0.3, 0.9]	0.796	0.55	0.5
OSTWR	0.15	[0.1, 0.35]	0.17	0.167	0.17
OSSOR	0.5	[0.18, 0.7]	0.628	0.633	0.627
OSBITHR	0.15	[0.1, 0.3]	0.12	0.14	0.12
TPMR	0.5	[0.4, 0.9]	0.86	0.7	0.59
MTH (mm)	4	[3, 5.5]	3.5	3.5	3.5

* PS-SPSS-SPMTM, PS-IPSS-SPMTM-1 and PS-SPSS-IPMTM-2 are the abbreviations for "partitioned stator single-phase short-stroke surface-mounted permanent magnet tubular machine", "partitioned stator single-phase short-stroke interior permanent magnet tubular machine 1" and "partitioned stator single-phase short-stroke interior permanent magnet tubular machine 2", respectively.

5. No-Load and Load Performance

Open-circuit flux distributions of the optimally designed machines are shown in Figures 7–9, when the flux linkage is maximum negative, zero, and maximum positive, respectively. It can be clearly seen that the direction and magnitude of the flux linkage change with the mover position. Moreover, all machines exhibit similar flux line patterns. However, PS-SPSS-IPMTM-2 suffers from high flux leakage at both ends, due to the PM location on both ends of its inner stator. The flux linkage variations with mover displacement of the three machines are compared in Figure 10. It shows that the PS-SPSS-IPMTM-2 has the highest flux linkage among the three machines. This is because it has the largest amount of PM usage in such a configuration. In contrast, the PS-SPSS-IPMTM-1 exhibits the lowest flux linkage, owing to the lowest PM volume. Figure 11 compares the profile of the back-EMF with the mover displacement. The highest back-EMF can be achieved by PS-SPSS-IPMTM-2 since it has the highest flux linkage.

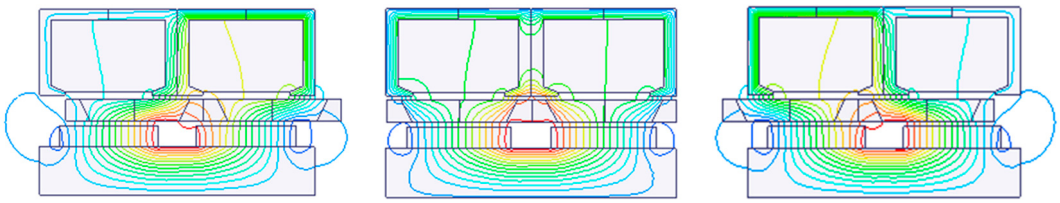

(**a**) (**b**) (**c**)

Figure 7. Open-circuit field distributions of PS-SPSS-SPMTM with different mover positions. (**a**) Position = −4 mm; (**b**) Position = 0; (**c**) Position = +4 mm.

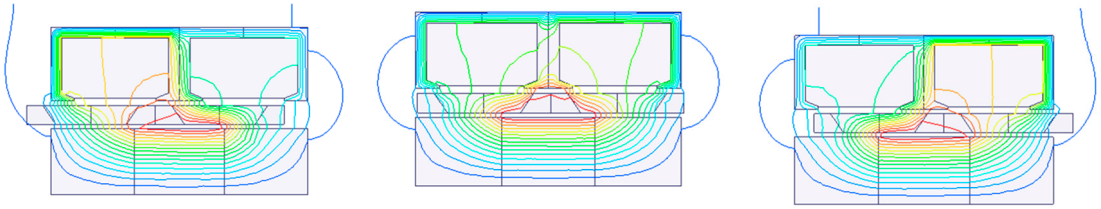

(**a**) (**b**) (**c**)

Figure 8. Open-circuit field distributions of PS-SPSS-IPMTM-1 with different mover positions. (**a**) Position = −4 mm; (**b**) Position = 0; (**c**) Position = +4 mm.

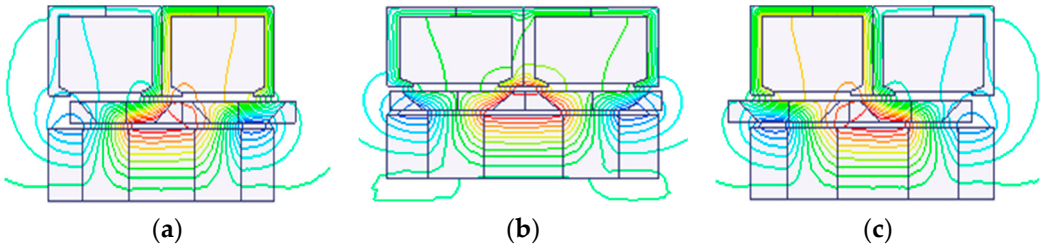

Figure 9. Open-circuit field distributions of PS-SPSS-IPMTM-2 with different mover positions. (**a**) Position = −4 mm; (**b**) Position = 0; (**c**) Position = +4 mm.

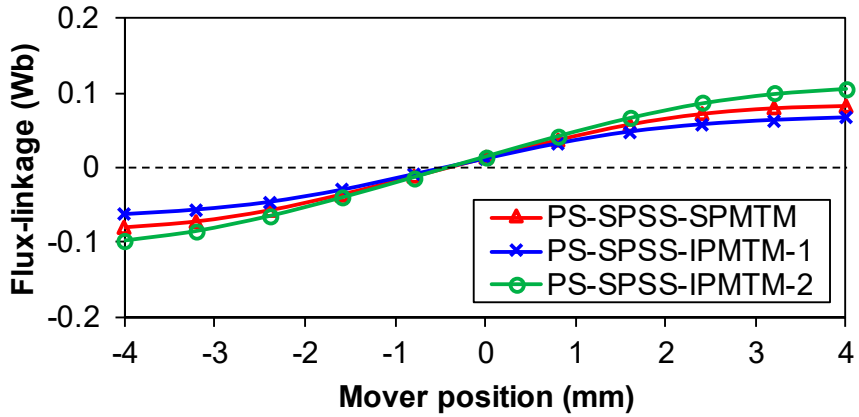

Figure 10. Comparison of flux linkages.

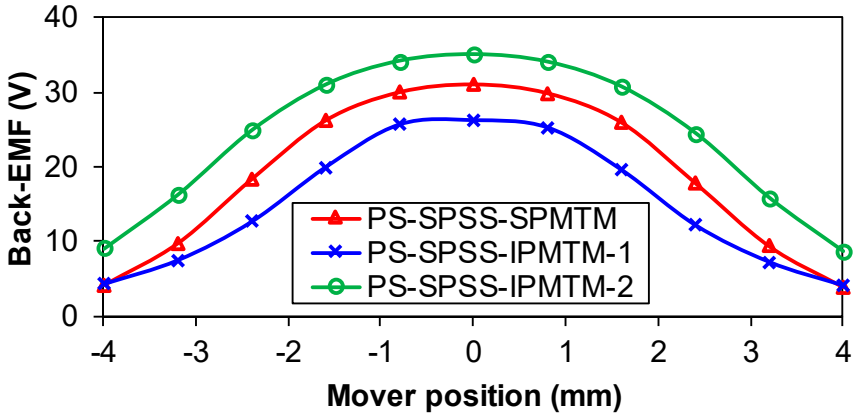

Figure 11. Comparison of back-EMFs.

Open-circuit cogging forces of the understudying machines, which may result in machine noise and vibration [36], are illustrated in Figure 12, whilst their thrust forces versus mover displacement are compared in Figure 13. It should be noted that the highest thrust force is obtained in PS-SPSS-IPMTM-2. PS-SPSS-SPMTM produces the lowest cogging force compared to PS-SPSS-IPMTM topologies, which is beneficial for applications requiring a smooth operation. Moreover, the lowest thrust force and the highest cogging force are observed in PS-SPSS-IPMTM-1.

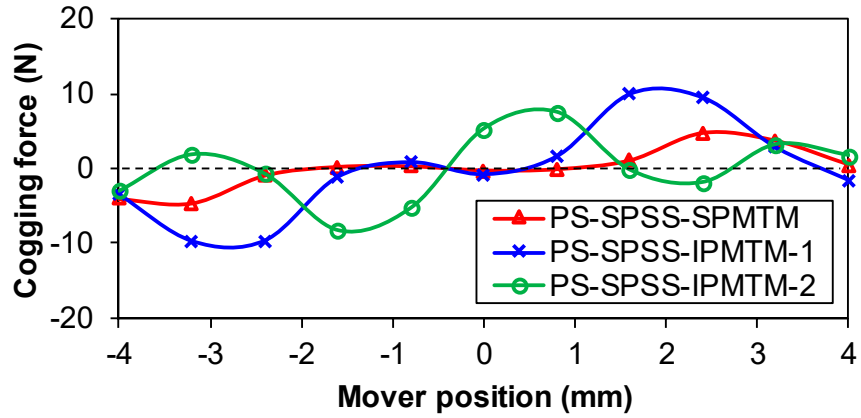

Figure 12. Comparison of cogging forces.

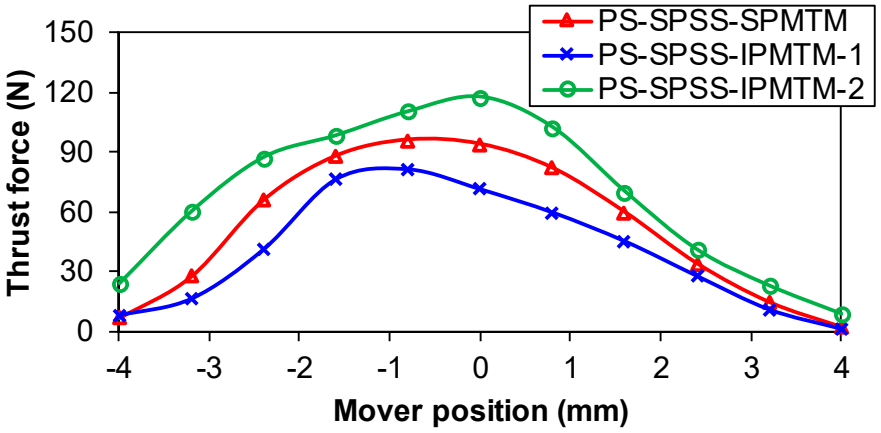

Figure 13. Comparison of thrust forces.

6. Comparison of Losses

Generally, an electrical machine's performance, particularly thermal behavior and efficiency, is strongly affected by losses. Therefore, losses should be taken into consideration. The iron loss is calculated using finite element software JMAG v19.1 (JSOL Corporation) [39] and both eddy current and hysteresis losses are included. The total iron loss consists of the iron losses in the inner and outer stators and the iron loss in the mover.

The iron core material of the outer stator is M300, while those of the inner stator and the mover are mild steel. The magnetization curves (BH curves) of the iron core materials are illustrated in Figure 14. It should be noted that the manufacturing assembly, such as modular structure and packing factor, has not been considered in the axisymmetric FEA calculation in this paper. However, the outer stator can be made of several modules laminated along the circumference, the same as in [40,41]. Iron loss variations with the velocity for all machines are compared in Figure 15. The highest iron loss is shown by the PS-SPSS-IPMTM-2. In contrast, the PS-SPSS-IPMTM-1 exhibits the lowest iron loss among the three topologies.

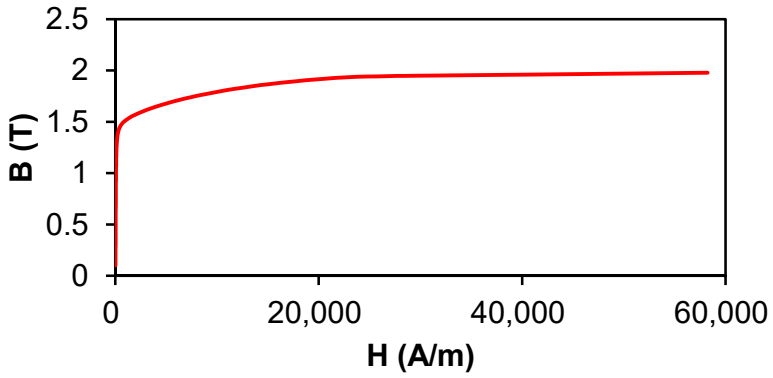

(**a**)

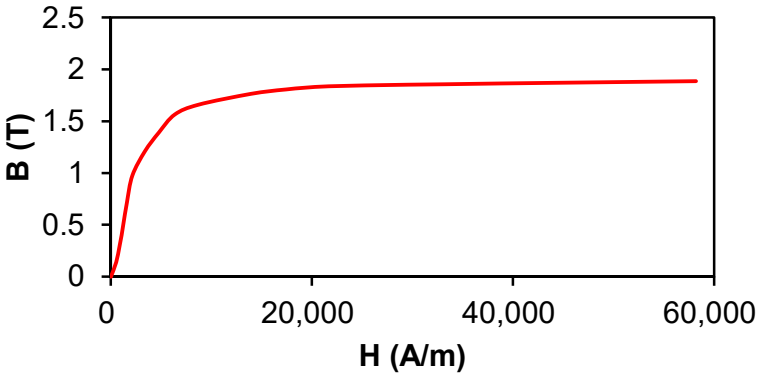

(**b**)

Figure 14. BH curves. (**a**) Outer stator; (**b**) Inner stator and mover.

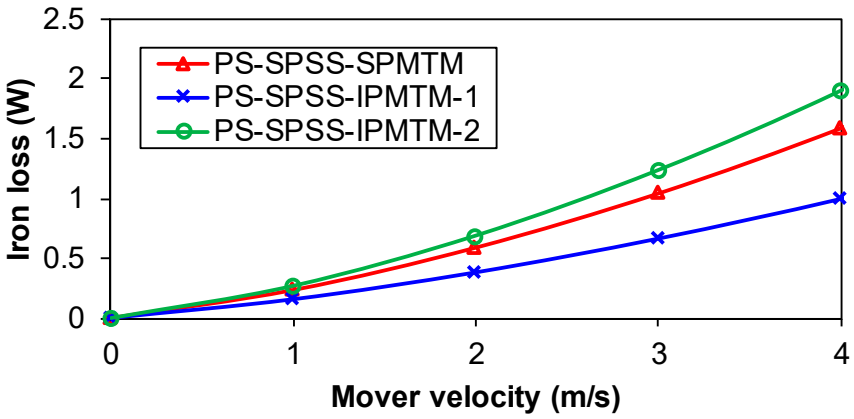

Figure 15. Comparison of iron losses under rated current density of 4 A/mm^2.

The PM eddy current loss is predicted based on the material property of N35SH (the resistivity is 1.4 $\times$ 10^{-6} Ω m). Figure 16 illustrates the magnet eddy current loss with the velocity for three machines. It can be seen that the proposed machines have very low magnet eddy current loss and both PS-SPSS-IPMT topologies have less magnet eddy current loss compared to that of PS-SPSS-SPMTM.

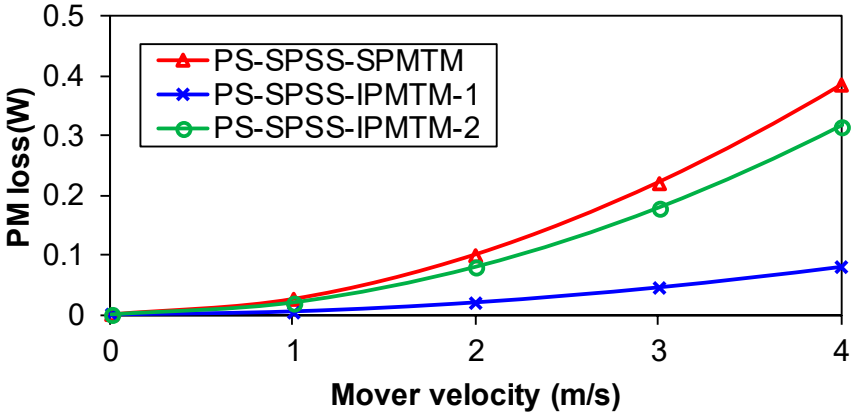

Figure 16. Comparison of PM eddy current losses under rated current density of 4 A/mm^2.

7. Comparison of PS-SPSS-SPMTM with a Conventional Single-Phase Short-Stroke Surface-Mounted Permanent Magnet Tubular Machine

The PS-SPSS-SPMTM and the conventional single-phase short-stroke surface-mounted PM tubular machine (SPSS-SPMTM) are compared in this section. The conventional SPSS-SPMTM consists of an E-shaped core stator with two annular windings, while the mover has two pole PMs with radial magnetization; see Figure 17. For a fair comparison, the conventional SPSS- SPMTM has been designed with the same major design parameters of the PS-SPSS-SPMTM. Furthermore, it has been globally optimized under the same optimization conditions of the PS-SPSS-SPMTM.

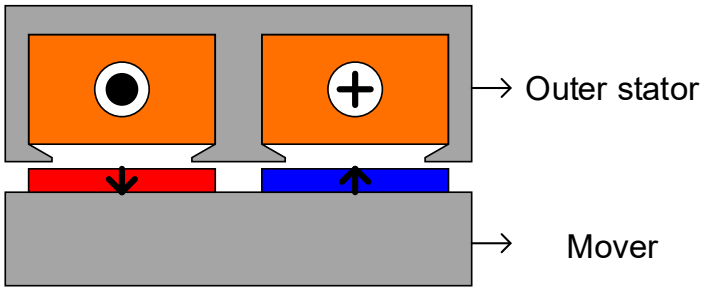

Figure 17. SPSS-SPMTM cross-section.

Table 4 illustrates the definitions of the varied parameters during the optimization and a schematic diagram of the main design parameters of the conventional machine is shown in Figure 18. SOR, SIR, STW, SSO, SBITH, and SSP represent the stator outer radius, the stator inner radius, the stator tooth width, the stator slot opening, the stator back iron thickness, and the stator slot pitch, respectively. TPM and MPP indicate the PM pole pitch and the mover pole pitch, respectively.

Table 4. Values of optimization parameters of single-phase short-stroke surface-mounted permanent magnet tubular machine (SPSS-SPMTM).

Symbols	Initials	Restrictions	Optimal
SR	0.5	[0.3, 0.75]	0.52
OSTWR	0.2	[0.1, 0.3]	0.185
OSSOR	0.5	[0.3, 0.9]	0.58
OSBITHR	0.15	[0.1, 0.3]	0.133
TPMR	1	[0.6, 1]	0.85

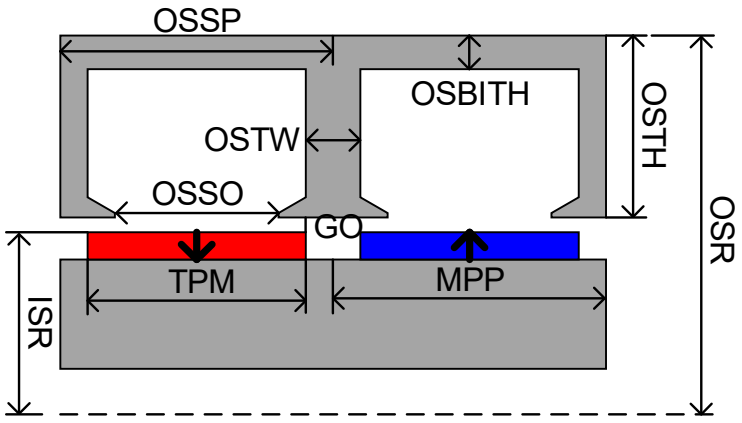

Figure 18. Major design parameters of SPSS-SPMTM.

Figure 19 shows flux distributions of the conventional SPM machine for three mover positions, i.e., at positive maximum, negative maximum, and zero flux linkages. It can be noted that although both the conventional and the proposed machines have similar flux distribution patterns, the proposed machine has higher flux leakage at the edges. Due to this, the conventional machine exhibits slightly more linear flux linkage variation compared to the proposed machine, as in Figure 20, and, consequently, flatter back-EMF, as in Figure 21. Furthermore, open-circuit cogging forces for both machines are compared in Figure 22. The proposed machine produces lower cogging force than the conventional machine, which is beneficial for applications requiring high reliability. Figure 23 illustrates thrust force variations with the displacement for both machines. It can be seen that the thrust force variation of the proposed machine is similar to its back-EMF profile. However, due to the cogging force effect, the thrust force-displacement characteristic profile of the conventional machine is different from its back-EMF profile. The conventional machine has a slightly higher thrust force at the center point compared to the proposed machine.

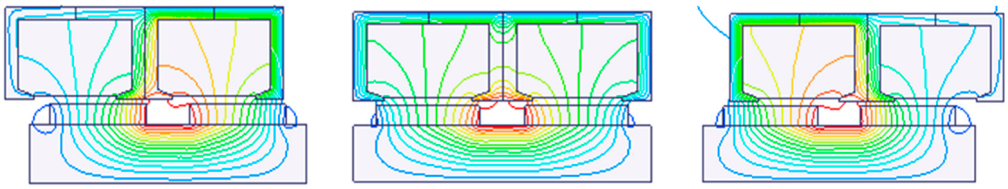

Figure 19. Open-circuit field distributions SPSS-SPMTM with different positions. (**a**) Position = −4 mm; (**b**) Position = 0; (**c**) Position = +4 mm.

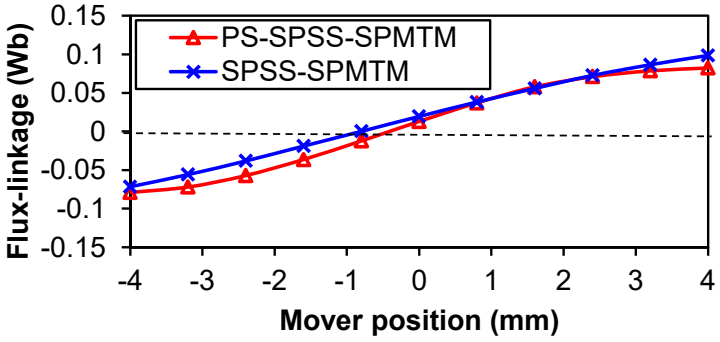

Figure 20. Comparison of flux linkages.

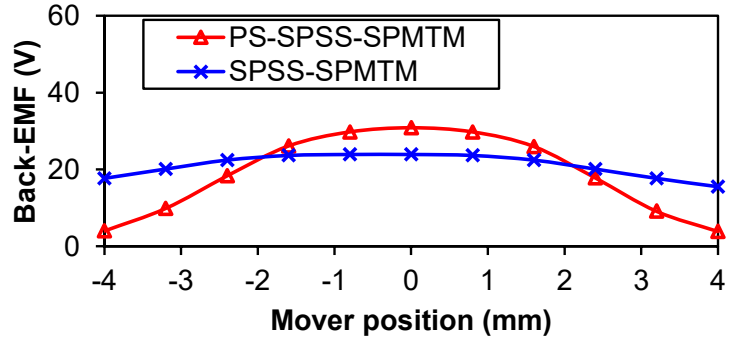

Figure 21. Comparison of back-EMFs.

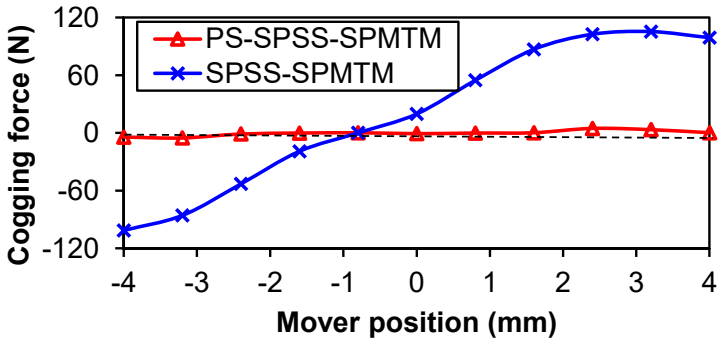

Figure 22. Comparison of cogging forces.

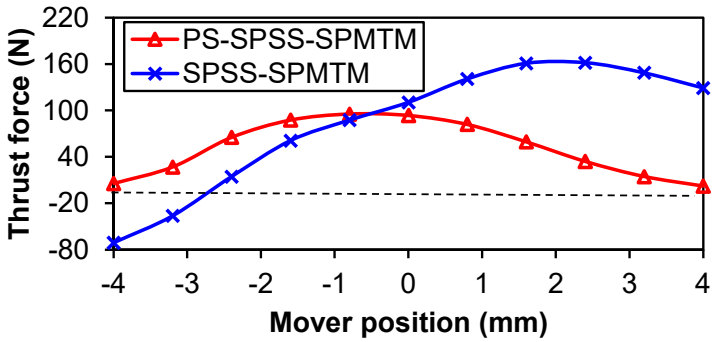

Figure 23. Comparison of thrust forces.

Iron loss variations with velocity for both machines at load condition are depicted in Figure 24. Both machines have low iron losses, although the proposed machine shows approximately 24% higher iron loss. Figure 25 illustrates the variations in magnet eddy current losses with velocity for both machines at load condition. It can be seen that the proposed machine has approximately 95% less magnet eddy current loss than the conventional machine. Hence, the potential problem in conventional machines, i.e., high PM temperature caused by eddy current loss, can be significantly improved by using a partitioned stator configuration. It is worth mentioning that at low velocity, the majority of linear machine losses are a result of copper loss. This is because such loss is frequency-independent. On the other hand, both iron and magnet eddy current losses will increase with the velocity.

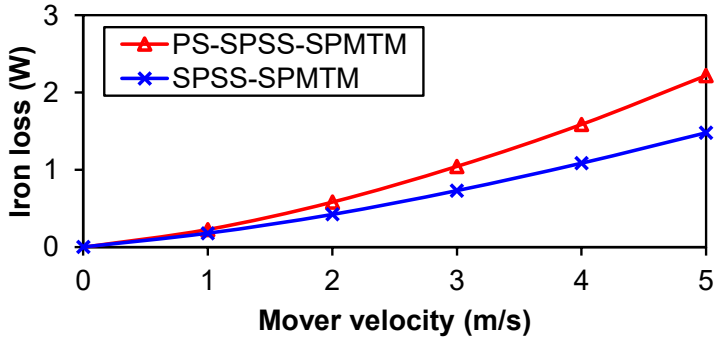

Figure 24. Comparison of iron losses under rated current density of 4 A/mm^2.

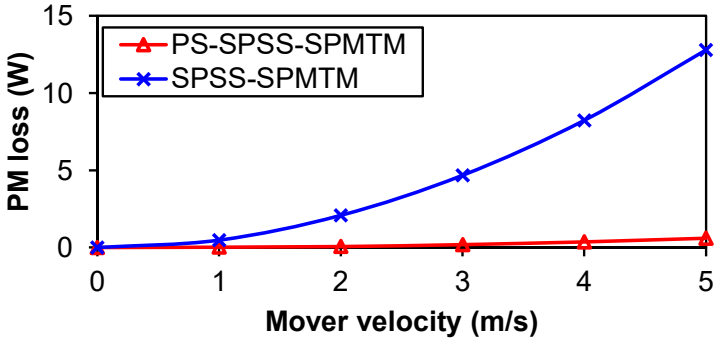

Figure 25. Comparison of PM eddy current losses under rated current density of 4 A/mm^2.

Table 5 summarizes the machines' performance. All the machines have the same volume. It can be seen that the SPSS-SPMTM consumes the lowest PM volume and delivers the highest thrust force and hence has the highest force per PM volume. The thrust force of the SPSS-SPMTM is 70% higher than its PS counterpart, whereas the mover mass of the former is four times that of the latter. Therefore, a much higher force to mass ratio is observed in PS-SPSS-SPMTM.

Table 5. Performance of compared machines.

Machines	SPSS-SPMTM	PS-SPSS-SPMTM	PS-SPSS-IPMTM-1	PS-SPSS-IPMTM-2
Total machine volume (cm^3)	181.64	181.64	181.64	181.64
PM volume (cm^3)	9.26	10.58	12.95	19.88
Mover mass (g)	609.9	146.87	146.87	146.87
Thrust force (Nm)	161.57	95.28	81.27	117.51
Force per PM volume (Nm/cm^3)	17.45	9.01	6.28	5.91
Force to mass ratio (Nm/g)	0.26	0.65	0.55	0.80

PS-SPSS-SPMTM consumes the lowest PM volume and delivers the second-highest thrust force among the three PS machines. Thus, this machine has a higher force per PM volume than the other two PS machines. It should be noted that PS-SPSS-IPMTM-2 has the highest force to mass ratio of 0.8, which is 200% higher than the SPSS-SPMTM.

8. Conclusions

Based on the partitioned stator concept, new SPSS-TPMOMs have been proposed in this paper. The influence of the PM poles' alignment with the stator teeth or stator slots is investigated. It is concluded that the PM poles must be aligned with the outer stator slots to obtain the oscillated movement of the mover in PS-SPSS-TPMOMs. Moreover, under the same design specification and optimization conditions, the proposed machines

have been optimized for maximum thrust force. The machines' performance is analyzed and compared.

It is observed that the proposed machines possess the merits of lighter mover mass and much lower magnet eddy current loss compared with the conventional SPSS-SPMTM. The PS-SPSS-SPMTM can achieve a comparable thrust force to that of the PS-SPSS-IPMTM-2; however, the magnet usage in such a topology is approximately 34% less compared to that of the PS-SPSS-IPMTM-2. Despite the fact that the PS-SPSS-IPMTM-1 has the lowest open-circuit and on-load performance among the three PS topologies, it shows the lowest iron as well as magnet eddy current losses compared to the other two PS machines.

Future work will include prototyping and experimental investigation, as well as system simulation for specific applications and 3D FEA considering a modular stator structure.

Author Contributions: Conceptualization, Z.-Q.Z. and Q.L.; methodology, Z.-Q.Z. and A.L.S.; software, A.L.S.; validation, formal analysis and investigation, Z.-Q.Z., A.L.S., Q.L., Y.L., H.Q.; resources, Z.-Q.Z.; data curation, A.L.S.; writing—original draft preparation, Z.-Q.Z. and A.L.S.; writing—review and editing, Q.L., Y.L., H.Q.; visualization, H.Q.; supervision, Z.-Q.Z.; project administration, Z.-Q.Z.; funding acquisition, Z.-Q.Z. All authors have read and agreed to the published version of the manuscript.

Funding: This research received no external funding.

Institutional Review Board Statement: Not applicable.

Informed Consent Statement: Not applicable.

Data Availability Statement: The data presented in this study are available on request from the corresponding author. The data are not publicly available due to confidentiality.

Conflicts of Interest: The authors declare no conflict of interest.

References

1. Lv, G.; Zhou, T.; Zeng, D.; Liu, Z. Design of ladder-slit secondaries and performance improvement of linear induction motors for urban rail transit. *IEEE Trans. Ind. Electron.* **2018**, *65*, 1187–1195. [CrossRef]
2. Cao, R.; Jin, Y.; Lu, M.; Zhang, Z. Quantitative comparison of linear flux-switching permanent magnet motor with linear induction motor for electromagnetic launch system. *IEEE Trans. Ind. Electron.* **2018**, *65*, 7569–7578. [CrossRef]
3. Cao, R.; Lu, M.; Jiang, N.; Cheng, M. Comparison between linear induction motor and linear flux-switching permanent-magnet motor for railway transportation. *IEEE Trans. Ind. Electron.* **2019**, *66*, 9394–9405. [CrossRef]
4. Lobo, N.S.; Lim, H.S.; Krishnan, R. Comparison of linear switched reluctance machines for vertical propulsion application: Analysis, design, and experimental correlation. *IEEE Trans. Ind. Appl.* **2008**, *44*, 1134–1142. [CrossRef]
5. Vatani, M.; Mirsalim, M. Comprehensive research on a modular-stator linear switched reluctance motor with a toroidally wound mover for elevator applications. In Proceedings of the International Power Electronics, Drive Systems and Technologies Conference (PEDSTC), Shiraz, Iran, 12–14 February 2019; pp. 61–66.
6. Wang, D.; Du, X.; Zhang, D.; Wang, X. Design, optimization, and prototyping of segmental-type linear switched-reluctance motor with a toroidally wound mover for vertical propulsion application. *IEEE Trans. Ind. Electron.* **2018**, *65*, 1865–1874. [CrossRef]
7. Kwon, Y.-S.; Kim, W.-J. Detent-force minimization of double-sided interior permanent-magnet flat linear brushless motor. *IEEE Trans. Magn.* **2016**, *52*, 1–9. [CrossRef]
8. Wang, H.; Li, J.; Qu, R.; Lai, J.; Huang, H.; Liu, H. Study on high efficiency permanent magnet linear synchronous motor for maglev. *IEEE Trans. Appl. Supercond.* **2018**, *28*, 1–5. [CrossRef]
9. Huang, X.Z.; Yu, H.C.; Zhou, B.; Li, L.Y.; Gerada, D.; Gerada, C.; Qian, Z.Y. Detent-force minimization of double-sided permanent magnet linear synchronous motor by shifting one of the primary components. *IEEE Trans. Ind. Electron.* **2020**, *67*, 180–191. [CrossRef]
10. Huang, X.Z.; Li, J.; Zhang, C.; Qian, Z.Y.; Li, L.; Gerada, D. Electromagnetic and thrust characteristics of double-sided permanent magnet linear synchronous motor adopting staggering primaries structure. *IEEE Trans. Ind. Electron.* **2018**, *66*, 4826–4836. [CrossRef]
11. Wang, J.B.; Howe, D. Analysis of an axially magnetized iron-cored tubular PM machine. *IET Proc. Electr. Power Appl.* **2004**, *151*, 144–150. [CrossRef]
12. El-Refaie, A.M. Fractional-slot concentrated-windings synchronous permanent magnet machines: Opportunities and challenges. *IEEE Trans. Ind. Electron.* **2020**, *57*, 107–121. [CrossRef]

13. Wang, J.; Howe, D.; Jewell, G.W. Analysis and design optimization of an improved axially magnetized tubular permanent-magnet machine. *IEEE Trans. Energy Convers.* **2004**, *19*, 289–295. [CrossRef]
14. Sui, Y.; Zheng, P.; Yu, B.; Cheng, L.; Liu, Z. Research on a tubular yokeless linear PM machine. *IEEE Trans. Magn.* **2015**, *51*, 8204904. [CrossRef]
15. Wang, J.; Jewell, G.; Howe, D. Design optimization and comparison of tubular permanent magnet machine topologies. *IET Proc. Electr. Power Appl.* **2001**, *148*, 456–464. [CrossRef]
16. Ji, J.; Yan, S.; Zhao, W.; Liu, G.; Zhu, X. Minimization of cogging force in a novel linear permanent-magnet motor for artificial hearts. *IEEE Trans. Magn.* **2013**, *49*, 3901–3904. [CrossRef]
17. Andriollo, M.; Dall'Ora, L.; Tortella, A. Electromagnetic parameter characterization of a short-stroke linear PM generator for renewable energy application. In Proceedings of the International Conference on Clean Electrical Power (ICCEP), Alghero, Italy, 11–13 June 2013; pp. 383–390.
18. Wang, J.; Howe, D.; Lin, Z. Analysis of a short-stroke, single-phase, quasi-Halbach magnetized tubular permanent magnet motor for linear compressor applications. *IET Electr. Power Appl.* **2008**, *2*, 193–200. [CrossRef]
19. Bai, J.; Fu, Z.; Yu, B.; Sui, Y.; Zhu, S.; Zheng, P. Design and optimization of a single-phase oscillating PM alternator used for free-piston stirling engines. In Proceedings of the 17th International Conference on Electrical Machines and Systems (ICEMS), Hangzhou, China, 22–25 October 2014; pp. 1738–1742.
20. Kim, C.-W.; Jang, G.-H.; Seo, S.-W.; Yoon, I.-J.; Lee, S.-H.; Jeong, S.-S.; Choi, J.-Y. Comparison of electromagnetic and dynamic characteristics of linear oscillating actuators with rare-earth and ferrite magnets. *IEEE Trans. Magn.* **2019**, *55*, 1–4. [CrossRef]
21. Bianchi, N.; Bolognani, S.; Corte, D.D.; Tonel, F. Tubular linear permanent magnet motors: An overall comparison. *IEEE Trans. Ind. Applicat.* **2003**, *39*, 466–475. [CrossRef]
22. Min, S.G.; Sarlioglu, B. A comparative study of coreless-type PM linear synchronous machines with non-overlapping windings. *IEEE Trans. Ind. Appl.* **2019**, *55*, 2481–2489. [CrossRef]
23. Wang, J.; Howe, D.; Lin, Z. Comparative study of winding configurations of short-stroke, single phase tubular permanent magnet motor for refrigeration applications. In Proceedings of the IEEE Industry Applications Annual Meeting, New Orleans, LA, USA, 23–27 September 2007; pp. 311–318.
24. Abdalla, I.; Ibrahim, T.; Nor, N. Comparative study of permanent magnet configurations of short-stroke linear motor for reciprocating compressor in household refrigerator application. *Inf. Technol. Electr. Eng.* **2013**, *2*, 16–24.
25. Ho, S.L.; Wang, Q.; Niu, S.; Fu, W.N. A novel magnetic-geared tubular linear machine with Halbach permanent-magnet arrays for tidal energy conversion. *IEEE Trans. Magn.* **2015**, *51*, 8113604. [CrossRef]
26. Chen, X.; Zhu, Z.Q.; Howe, D.; Dai, J. Comparative study of alternative permanent magnet linear oscillating actuators. In Proceedings of the International Conference on Electrical Machines and Systems, Wuhan, China, 17–20 October 2008; pp. 2826–2831.
27. Li, X.; Xu, W.; Ye, C.; Zhu, J. Novel hybrid-flux-path moving-iron linear oscillatory machine with magnets on stator. *IEEE Trans. Magn.* **2017**, *53*, 1. [CrossRef]
28. Shuheng, Q.; Jie, Z.; Chi, Z. Effects of Halbach and non-Halbach arrays on thrust characteristics of ironless permanent magnet linear motors: A simulation and optimization. In Proceedings of the International Conference on Electrical Machines and Systems, Hamamatsu, Japan, 24–27 November 2020; pp. 1659–1662.
29. Souissi, A.; Abdennadher, I.; Masmoudi, A. Comparison of the no-load features of IPM and consequent pole tubular-linear PM synchronous machines. In Proceedings of the Fourteenth International Conference on Ecological Vehicles and Renewable Energies (EVER), Monte-Carlo, Monaco, 8–10 May 2019; pp. 1–8.
30. Cao, R.; Cheng, M.; Mi, C.C.; Hua, W. Influence of leading design parameters on the force performance of a complementary and modular linear flux-switching permanent-magnet motor. *IEEE Trans. Ind. Electron.* **2014**, *61*, 2165–2175. [CrossRef]
31. Zhao, W.; Cheng, M.; Hua, W.; Jia, H.; Cao, R. Back-EMF harmonic analysis and fault-tolerant control of flux-switching permanent-magnet machine with redundancy. *IEEE Trans. Ind. Electron.* **2011**, *58*, 1926–1935. [CrossRef]
32. Cao, R.; Cheng, M.; Hua, W. Investigation and general design principle of a new series of complementary and modular linear FSPM motors. *IEEE Trans. Ind. Electron.* **2013**, *60*, 5436–5446. [CrossRef]
33. Zhao, W.; Cheng, M.; Chau, K.T.; Cao, R.; Ji, J. Remedial injected harmonic current operation of redundant flux-switching permanent magnet motor drives. *IEEE Trans. Ind. Electron.* **2013**, *60*, 151–159. [CrossRef]
34. Cheng, M.; Hua, W.; Zhang, J.; Zhao, W. Overview of stator permanent magnet brushless machines. *IEEE Trans. Ind. Electron.* **2011**, *58*, 5087–5101. [CrossRef]
35. Zheng, P.; Sui, Y.; Tong, C.; Bai, J.; Yu, B.; Lin, F. A novel single-phase flux-switching permanent magnet linear generator used for free-piston stirling engine. *J. Appl. Phys.* **2014**, *115*, 1–3. [CrossRef]
36. Zheng, P.; Sui, Y.; Yu, B.; Cheng, L.; Wang, W. A tubular single-phase dual-stator flux-switching PM oscillating generator with series magnetic circuit. In Proceedings of the IEEE International Magnetics Conference, Beijing, China, 11–15 May 2015; p. 1.
37. Chen, X.; Zhu, Z. Modelling and evaluation of linear oscillating actuators. *J. Int. Conf. Electr. Mach. Syst.* **2012**, *1*, 517–524. [CrossRef]
38. Wang, M.; Li, L.; Pan, D. Detent force compensation for pmlsm systems based on structural design and control method combination. *IEEE Trans. Ind. Electron.* **2015**, *62*, 6845–6854. [CrossRef]

39. Sano, H.; Narita, K.; Asanuma, T.; Yamada, T. An accurate iron loss evaluation method based on finite element analysis for permanent magnet motors. In Proceedings of the 2016 XXII International Conference on Electrical Machines (ICEM), Lausanne, Switzerland, 4–7 September 2016; pp. 1284–1289.
40. Hor, P.J.; Zhu, Z.Q.; Howe, D.; Rees-Jones, J. Eddy-current loss in a moving-coil linear tubular permanent magnet brushless motor. *IEEE Trans. Magn.* **1999**, *35*, 3601–3603. [CrossRef]
41. Wang, J.; Howe, D. Influence of soft magnetic materials on the design and performance of tubular permanent magnet machines. *IEEE Trans. Magn.* **2005**, *41*, 4057–4059. [CrossRef]